UC Santa Barbara
UC Santa Barbara Previously Published Works

Title

Modeling human health characterization factors for indoor nanomaterial emissions in life cycle assessment: a case-study of titanium dioxide

Permalink

https://escholarship.org/uc/item/74x5j7vp

Journal

Environmental Science Nano, 4(8)

ISSN

2051-8153

Authors

Tsang, Michael P
Li, Dingsheng
Garner, Kendra L
et al.

Publication Date

2017

DOI

10.1039/c7en00251c

Peer reviewed

PAPER

Modeling human health characterization factors for indoor nanomaterial emissions in life cycle assessment: a case-study of titanium dioxide†

Michael P. Tsang, [ab] Dingsheng Li, [c] Kendra L. Garner, [cd]
Arturo A. Keller, [cd] Sangwon Suh [cd] and Guido W. Sonnemann [*ab]

Life cycle assessment is used during the developmental stages of products and technologies. In the case of emerging technologies such as engineered nanomaterials there are limitations in using life cycle assessment to evaluate the direct environmental and human health impacts from emissions of nanomaterials themselves. This is due to the limited life cycle inventory data and life cycle impact assessment models currently available for describing the fate, exposure and effects of engineered nanomaterials in the environment. Specifically, current life cycle impact assessment methodologies do not include characterization factors for nanomaterials. Engineered nanomaterials may be emitted throughout the life cycle of a product, for example, in the occupational setting where there may be constant interaction between workers and large volumes of loose nano-powders. This paper presents a dynamic model that is intended for use in life cycle impact assessment methods to quantify the fate, exposure and human health effects of engineered nanomaterials. Using the case-study of nano-TiO_2 emissions in the indoor workplace, nano-specific life cycle assessment characterization factors are presented. Compared to previously published steady-state models, the results of the current study demonstrate a much lower exposure potential, expressed as the 'retained'-intake fraction of nano-TiO_2 in the lung over the total emitted amount. Furthermore, the results indicate that smaller emissions lead to greater fractional deposition. Thus, an inverse relationship between the total indoor air emissions of nano-TiO_2, and the resulting magnitude of the characterization factor was seen.

Environmental significance

Nanomaterials possess an endless range of possible sizes, shapes, types and compositions that are being used to drive the development and production of new and emerging technologies. Concurrently, this these materials pose potential ecological and human health hazards if emitted into the environment. Moreover, their new and varied properties introduce challenges to existing tools such as life cycle assessment that aim to identify and minimize a product's negative impact on the environment. This paper presents an approach and discusses the findings of trying to introduce dynamic fate and exposure modeling into life cycle impact assessment methods in order to address the current gap in human health impacts from indoor air emissions of engineered nanomaterials in life cycle assessment.

1. Introduction

Engineered nanomaterials (ENM) provide benefits across many sectors,[1] but they also raise concerns regarding poten-

^{a} ISM, UMR 5255, Univ. Bordeaux, F-33400 Talence, France.
E-mail: guido.sonnemann@u-bordeaux.fr
^{b} CNRS, ISM, UMR 5255, F-33400 Talence, France
^{c} Bren School of Environmental Science & Management, University of California, Santa Barbara, CA 93106-5131, USA
^{d} Center for Environmental Implications of Nanotechnology (UC CEIN), University of California, Santa Barbara, CA, USA

† Electronic supplementary information (ESI) available. See DOI: 10.1039/c7en00251c

tial environmental and human health hazards.[2–4] While nanotechnologies can be evaluated with life cycle assessment (LCA) to determine their potential resource efficiencies and environmental and human health impacts, LCA does not evaluate the direct environmental and human health hazards posed by ENM emissions across their life cycles.[5,6] While it is possible to build life cycle inventories (LCI) that estimate and quantify ENM emissions,[7–10] currently available life cycle impact assessment (LCIA) methodologies do not cover nano-specific characterization factors (CF) that are necessary for quantifying the fate of, exposure to, and impacts from those emissions in an LCA.[11] A few studies have made first approximations to define nano-specific CF,[12–16] but otherwise the

direct impacts from ENMs have not been addressed by past LCA studies on ENMs.[14,17] Additionally, ambient (*i.e.* outdoor) emissions have historically been the focus of LCIs,[18] as is reflected in the scope of nano-specific CFs published to date. However, indoor emissions, particularly in occupational settings, can be important contributors to the overall LCA results.[18–22] Neglecting such emissions and their potential impacts in an LCA may result in burden shifting from the environment to workers.

Currently, LCIA models exploit several assumptions that describe the fate and transport of small organic molecules and metals well, but these methods are not appropriate for ENMs.[23] Traditional characterization models assume steady-state conditions or thermodynamic equilibrium,[24,25] ignoring the changes in concentration of the pollutant over time. Therefore, these models rely on (equilibrium) partition coefficients (*e.g.* octanol–water partition coefficient, K_{ow}) for estimating the fate of pollutants.

However, ENMs behave like colloidal substances that exist in their own phase when released into a specific medium.[26] Therefore, ENMs are not thermodynamically stable, even if some may be kinetically stable for long periods of time.[23] In other words, ENM concentration ratios between two mediums cannot be predicted from a previously measured partition coefficient after the further addition or removal of ENMs from that system.[23] Instead, the behavior of ENMs in the environment is concentration dependent. Consequently, their behavior in the environment can be estimated kinetically using dynamic models that describes the rates of the processes that control their behavior,[13,23] such as homo- and hetero-aggregation[27] or even clearance and retention from an organism.[28–30] While recent adaptations to existing LCIA models have been made to estimate both ecotoxicity[12–14,16] and human health toxicity[15,16,31] impacts, steady-state assumptions were used in all cases.

Thus, the aim of this paper is to present a dynamic model for estimating the human health impacts of ENMs in occupational, indoor environments. While previous studies have looked at the ambient emissions and impacts to the environment from mainly risk assessment perspectives,[27,32,33] this paper focuses specifically on LCIA methods for calculating the impacts of occupational, indoor air ENM emissions due to the potential exposure to uniquely high volumes of these materials. The approach presented in this paper is applied to nano-TiO$_2$, which is an ENM produced and used in high volumes globally and across many industries.[34–38]

2. Methods

A dynamic LCIA model is presented for calculating the human health impacts from occupational, indoor air emissions of metal oxide nanoparticles, with a focus on nano-TiO$_2$. Specifically, a CF (eqn (1)) for use in LCA is defined as follows:[39,40]

$$CF_{i,j} = iF_{i,j} \cdot EF_i \quad (1)$$

The CF is based on the concept proposed in USEtox[39,41] for calculating the human health life cycle impacts resulting from the emission of a substance (i) in a specific exposure scenario (j), given its intake fraction (iF) and its effect factor (EF). The iF represents the ratio of the mass of substance to which one is exposed per mass of the total emitted substance. The EF is defined by the toxicological dose–response relationship of the substance. Unlike in USEtox, the iF in this paper is not estimated using (equilibrium) partition coefficients characteristic of steady-state models. Instead, a retained-intake fraction (RiF) was derived from a dynamic fate and exposure models described in further detail in the following sections.

2.1 Exposure scenarios and occupational, indoor air emissions of nano-TiO$_2$

A total of 6 exposure scenarios (ES1–ES6) were modeled based on a previous occupational risk assessment involving nano-TiO$_2$.[42] These 6 scenarios were variations of a single representative workplace-activity involving the handling of nano-TiO$_2$ (Table 1).

The exposure scenarios were adapted from a single scenario from the NANEX (www.nanex-project.eu) database. These scenarios describe a situation where pre-fabricated nano-TiO$_2$ were handled, poured and transferred into large vessels. Thus, these scenarios do not estimate exposure during the production of nano-TiO$_2$. Potential emissions during production were not included based on the assumption that the manufacture of ENMs is more likely to occur under automated, enclosed settings where fugitive (*i.e.* accidental) exposures were near zero. Emissions rates (E, mg min^{-1}) were estimated as a function of the total mass of nano-TiO$_2$ handled ($A_{handled}$, kg), the dustiness index (DI, mg of dust per kg of material) of nano-TiO$_2$ and the handling energy factor (H, *unit-less*) of the work-related activity (eqn (2)).[43]

$$E_{i,j} = \frac{A_{handled,j}}{t_{wc,j}} \cdot (DI_i) \cdot (H_j), \quad (2)$$

t_{wc} is the duration (min) of the work activity and the DI for nano-TiO$_2$ was defined as 15 mg kg^{-1}.[42] H is based on a scale of 0–1, whereby 0 is a no-energy event (*e.g.* no handling of the material) and 1 is a high energy event (*e.g.* dropping from greater than a height of 2 m).[44]

The exposure scenarios represent variations of the same handling activity defined by differences in (a) the emission rate, E, and (b) the frequency of the work-cycle activity, f (*i.e.* a function of both duration and length of emission). ES1, ES2, ES3 and ES4 all had the same emission rates but at varying frequencies of 60 min emission events (*i.e.* work-cycle) with 60 minute pauses in between, 480 min all-day emission events with no pauses, and 1 min emission events with an indefinite pause the remainder of the workday, respectively. Compared to ES1 whose frequency of 10 min was defined as short, ES2, ES3 and ES4 represent long, daily (*i.e.* non-

Table 1 Parameters used in the emissions and fate and transport models describing the exposure scenarios where various amounts of nano-TiO$_2$ powder are transferred into a vessel. The exposure scenarios were defined by the magnitude of the emission per minute, E, and the frequency of the work-cycle activity, f, the handling energy factor, H, the work cycle time (*i.e.* duration of the work-related activity), t_{wc}, the pause between work cycles, p_{wc}, the number of work cycles, n_{wc}, the amount of material transferred per transfer event within each work cycle, $A_{handled}$, the total volume of the work room, V_{tot}, and the air exchange rate of the work-room AER

No.	Exposure scenario	$E_{i,j}$ [mg min^{-1}]	H_j	$t_{wc,j}$ [min]	$p_{wc,j}$ [min]	$n_{wc,j}$	$A_{handled,j}$ [kg]	$V_{tot,j}$ [m^3]	AER$_j$ [h^{-1}]
ES1	e-high, *f-short*	6.72×10^2	0.80	10	20	16	5.60×10^2	100	8
ES2	e-high, *f-long*	6.72×10^2	0.80	60	60	4	3.36×10^3	100	8
ES3	e-high, *f-daily*	6.72×10^2	0.80	480	0	1	2.69×10^4	100	8
ES4	e-high, *f-single pulse*	6.72×10^2	0.80	1	0	1	5.60×10	100	8
ES5	e-medium, *f-short*	6.72×10	0.80	10	20	16	5.60×10	100	8
ES6	e-low, *f-short*	6.72×10^{-2}	0.80	10	20	16	5.60×10^{-2}	100	8

e: Refers to an abbreviation of the emission rate, E, specifically for categorizing and naming the exposure scenarios.

interrupted) and single-pulse frequencies, respectively. Conversely, ES5 and ES6 had the same emission frequencies as ES1 but modified emission rates that were 2- and 4-orders of magnitude smaller than ES1, respectively. Compared to ES1 whose emission rate was considered high, ES5 and ES6 were considered medium and low rates, respectively. Emissions, according to the work-related activities described for ES1–ES6, were assumed to take place during an 8 hour work period, 5 days a week, 50 weeks per year (*i.e.* 2 weeks of holiday and time off, apart from weekends).

2.2 Fate and transport of airborne nano-TiO$_2$

In this paper, a two-zone, dynamic fate and transport model is presented for use with indoor, occupational ENM airborne emissions (Fig. 1).

A single emission source was modeled located inside a near-field (NF) zone. The remaining indoor air room volume was defined as the far-field (FF) and should not be confused with outdoor air volumes. The NF is defined as the volume of a hemisphere with a radius of 0.8 m. This radius corresponds to being an arm's length away from the source of emission[44]

and relevant given the workplace activities described in ES1–ES6. Both NF and FF zones were modeled as well-mixed compartments connected by advective air flow.[45] Existing LCA indoor air LCIA methods utilize a one-box model under the assumption that there is only one emission source in a well-mixed room[46] (eqn (3)):

$$V_j \cdot \frac{dC_{i,j}}{dt} = E_{i,j} - \left(C_{i-1,j} \cdot Q_j \right) \tag{3}$$

where V is the volume (m^3) of the compartment (*i.e.* the one-box), C_i is the concentration at a given time-step (µg m^{-3}), C_{i-1} is the concentration at the previous time-step and Q is the ventilation rate (m^3 h^{-1}). In the case of indoor air emissions from single point sources, it can be anticipated that large concentration gradients will exist between the point of emission and points further away from the source.[47] To accommodate for imperfect mixing, LCIA methods can use a mixing factor, m (eqn (4)).[20,31,39,46]

$$V_j \cdot \frac{dC_{i,j}}{dt} = E_{i,j} - \left(C_{i-1,j} \cdot Q_j \cdot m_j \right) \tag{4}$$

However, the use of m may result in underestimations of NF exposure upwards of 50% compared to the results of a two-zone model.[45,47] Thus, in this paper a two-zone model was used to address the difference between NF (eqn (5)) and FF (eqn (6)) concentrations of airborne nano-TiO$_2$.

$$V_{NF,j} \cdot \frac{dC_{NF,i,j}}{dt} = E_{i,} + \left(\beta_j \cdot C_{FF-1,i,j} \right) - \left(C_{NF-1,i,j} \cdot Q_j \right) - \left(\beta_j \cdot C_{NF-1,i,j} \right) \tag{5}$$

$$V_{FF,j} \cdot \frac{dC_{FF,i,j}}{dt} = \left(\beta_j \cdot C_{NF-1,i,j} \right) - \left(C_{FF-1,i,j} \cdot Q_j \right) - \left((\beta_j + Q_j) \cdot C_{FF-1,i,j} \right) \tag{6}$$

β is the inter-zonal advective exchange rate (m^3 min^{-1}) connecting the NF and FF air volumes. It was defined as the
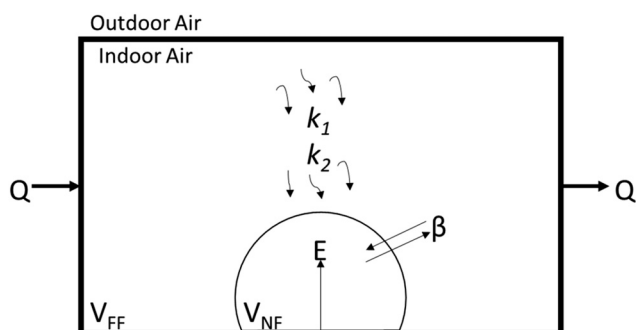

Fig. 1 Representation of the model used to estimate the emissions (E) and characterize the fate and transport of nano-TiO$_2$ in an indoor, two-zone occupational exposure scenario. The fate and transport model accounts for interzonal air transfer (β) between the NF and FF, air exchange (Q) between the indoor and outdoor air as well as non-advective sources of fate (k_i) such as aggregation and gravitational settling.

volume of air entering and leaving through half of the curved surface area of a hemisphere, whose radius, r (m), was equal to that of the NF, and the average air speed (m s^{-1}) between the NF and FF, s (eqn (7)).[45]

$$\beta_j = s_j \cdot \pi \cdot r_{NF,j}{}^2 \qquad (7)$$

ENMs settle out of the air at a relatively slow rate,[48] thus when indoor ENM emissions rates are sufficiently low and ventilation rates are high, steady-state ventilation models may adequately describe particle loss and estimate indoor ENM concentrations.[31] However, these conditions may not always be met, as has been demonstrated for organic chemicals.[40] For ENMs, this means other non-advective sources of particle loss such as homo- and hetero-aggregation and gravitational settling should be considered.[31] The introduction of non-advective sources of particle loss (k) in a two-zone, dynamic model is represented by eqn (8) and (9).

$$V_{NF,j} \cdot \frac{dC_{NF,i,j}}{dt} = E_{i,j} + \left(\beta_j \cdot C_{FF\text{-}1,i,j} \right) - \left(C_{NF\text{-}1,i,j} \cdot V_{NF,j} \cdot \sum k_z \right) - \left(\beta_j \cdot C_{NF\text{-}1,i,j} \right)$$
$$(8)$$

$$V_{FF,j} \cdot \frac{dC_{FF,i,j}}{dt} = \left(\beta_j \cdot C_{NF\text{-}1,i,j} \right) - \left(C_{FF\text{-}1,i,j} \cdot V_{FF,j} \cdot \sum k_z \right) - \left(\left(\beta_j + Q_j \right) \cdot C_{FF\text{-}1,i,j} \right)$$
$$(9)$$

where k is any process of non-ventilation (z) removal, V_{NF} is the near field volume and V_{FF} is the far field volume. Non-ventilation particle losses considered in this model are (i) homo- and hetero-aggregation, herein referred to as aggregation, and (ii) gravitational settling. Aggregation was estimated using a first order rate constant (k_h) of 9.4×10^{-5} min^{-1}.[27] The removal, k_{set}, due to gravitational settling, based on Stokes' Law, is defined by eqn (10):

$$k_{set,z} = \frac{v_{set,i}}{h_j} = \left[\frac{\rho_{p,i} \cdot d_{e,i}{}^2 \cdot g \cdot C_{s,i}}{18 \cdot n \cdot x_i} \right] \left[\frac{1}{h_j} \right] \qquad (10)$$

where v_{set} is the settling velocity (m min^{-1}), ρ_p is the particle density (kg m^{-3}), $d_e{}^2$ is the equivalent volume diameter (nm), g is the gravitational force, C_S is the Cunningham slip correction factor (unit-less),[49] n is the viscosity of the medium (kg m^{-1} min^{-1}), x is the dynamic shape factor (unit-less, *i.e.* perfectly spherical materials have a value of 1), and h is the height (m) of the emission source. Gravitational settling is likely to be more important for ENMs and aggregates that are ≥100 nm, while Brownian motion might be more important for ENMs below 100 nm, although this distinction is not absolute and may differ based on the properties of the ENM under consideration.[29,31,50] Particles that deposit onto surfaces could potentially be re-suspended, attach to the skin upon contact from a surface or be removed by cleaning (*e.g.* sweep-

ing). It was assumed that there was no direct contact to contaminated surfaces with the skin and that all of the nano-TiO$_2$ deposited onto the ground was cleaned each day and not allowed to accumulate. All the parameters and their corresponding values that were used to run the fate and transport model are listed in Table 2. The model was constructed in MatLab 9.0 (MathWorks, USA).

2.3 Exposure to occupational indoor air concentrations of nano-TiO$_2$

Regarding human exposure to ENM, emissions may be taken up by inhalation, through direct contact with skin, or ingestion. While all routes of exposure are important to consider, this study focuses on the inhalation of airborne nano-TiO$_2$ in the occupational setting. Exposure during work-related activities was assumed to occur only in the NF, while workers were assumed to be exposed in the FF during non-work cycles (*i.e.* pause cycles). A physiologically-based pharmacokinetic (PBPK) model was adapted from Li *et al.*[28] to establish the deposition and retention of nano-TiO$_2$ in the lung over time. This model was originally built to estimate the exposure of inhaled cerium oxide nanoparticles in rats, and was adapted for human-based PBPK modeling upon inhalation of nano-TiO$_2$ using human-relevant parameter values for human, adult, male lungs (see ESI†).[53–58] The reader is referred to Li *et al.*[28] for complete details on the model, but a brief explanation follows.

The overall exposure model does not consider the use of personal protective equipment (PPE) but assumes direct interaction between the airways and indoor air. The MPPD v3.01 dosimetry model was used to derive values of regional (fractional) ENM deposition in the lungs (see ESI†).[59] Because MPPD v3.01 does not model deposition and clearance under variable exposure conditions, MPPD data was fed into the PBPK model to estimate bio-distribution in the lung. The PBPK model estimated the final retention in the lung after considering (i) mucociliary clearance, (ii) phagocytosis and (iii) translocation of nano-TiO$_2$ into systemic circulation.[28] The model estimated deposition in (i) the head or upper airways, (ii) the tracheobronchial region, and (iii) the pulmonary regions of the lung (*i.e.* air exchange occurs at the alveoli). Flow- and diffusion-limited processes, defined by permeability and partition coefficients (not to be confused by partition coefficients previously discussed for steady-state fate and transport modeling), governed the exchange of ENMs with blood and tissues (see ESI†). PCs had organ-specific saturation levels that limited their rate of ENM sequestration as PCs reached saturation. Finally, the mucociliary clearance rate was defined as a constant, irrespective of ENM loading in the lung. It was shown that pulmonary clearance of particulates is 10 times faster in rats compared with humans.[60] This might be partially explained by the greater mucociliary clearance rate in rats compared to humans. Thus, the transport factor governing translocation of loaded-PCs to the tracheobronchial region was defined as 1.44×10^{-6} min^{-1}, which

Table 2 Parameters and their values used in the fate and transport model that describes the occupational workplace settings for ES1–ES6

Parameter	Description	Value	Units	Additional information
r	Radius of near-field	0.80	m	Average arm's length from emission source[44]
V_{NF}	Volume of the near-field	1.07	m^3	Volume of a hemisphere with radius, r
V_{FF}	Volume of the far-field	98.9	m^3	Defined as $V_{tot} - V_{NF}$, where V_{tot} is 100 m^3
β	Inter-zonal air flow	21.9	$m^3\ min^{-1}$	Eqn (7)
s	Air flow between near- and far-fields	0.18	$m\ s^{-1}$	Calculated from reported (measured) indoor air speeds at occupational workplaces dealing with powder mixers and packers, excluding the outlier (see ESI)[51]
$k_{h,a}$	Aggregation rate constant	9.4×10^{-5}	min^{-1}	First-order rate constant in air[27] assumed for both homo- and hetero-aggregation.
v_{set}	Gravitational settling based on Stoke's law	N/A	$m\ min^{-1}$	Eqn (10)
ρ_p	ENM particle density	3900	$kg\ m^{-3}$	33
d_e	Diameter of ENM	21.0	nm	Equivalent volume diameter
g	Gravitational acceleration	9.8	$m\ s^{-2}$	
C_s	Cunningham slip correction factor	1.0	Unit-less	(see ESI)[52]
n	Viscosity of air	1.1×10^{-3}	$kg\ m^{-1}\ min^{-1}$	33
x	Dynamic shape factor	1.0	Unit-less	Values of 1 for perfectly spherical particles
h_w	Height of the workplace	2.50	m	43
h_e	Height of the emission source	1.6	m	Interpreted from the handling energy factor of 0.8, whereby a value of 1 means a drop height greater than 2 meters.[43]
T	Time scale	10 080	min	Number of minutes in a week
t	Time-step	1	min	Time resolution at which the model was integrated
AER	Air-exchange rate	8.0	h^{-1}	In a two-zone model, this represents the air exchange rate of the far-field room volume[43]

is one order of magnitude slower than reported by Li *et al.*[28] Exposure was expressed as total wet lung burden and reported as an internal mass dose of nano-TiO$_2$ per mass of wet lung. The wet lung was defined as the pulmonary and interstitial regions of the lung and the corresponding blood and PCs found in those compartments, while excluding the upper airway and trachea–bronchial regions. The PBPK model was implemented in Berkeley Madonna™ version 8.3.23 (Berkeley, CA).

2.4 Retained-intake fraction of nano-TiO$_2$ emissions to occupational indoor air

The emissions and resulting exposures were combined into an overall RiF, which represents a ratio of the average internal wet lung mass dose of TiO$_2$ (EXP$_{int}$) per average lifetime emitted mass of TiO$_2$ (E_{life}). This is different from traditional inhalation iF, which is the inhaled amount per emitted amount.[61] Two different time-horizons were used to represent limited (*i.e.* 'acute') and chronic exposures, defined using a (i) 1 year and (ii) 45 year (*i.e.* lifetime) work period, respectively. The time-weighted average wet lung burdens were calculated over an assumed life expectancy of 70 years, defined by periods of (i) non-work years from 1–20, (ii) work years from 21–65 and (iii) non-work in their retirement years from 66–70. Thus, the model assumed emissions that occurred according to the working conditions described in section 2.1 (*i.e.* emissions during working hours and workdays) throughout a pre-defined set of working years between ages 20–65 irrespective of whether the person was employed for the 1 year or 45 years. Therefore, the 1 year time-weighted lung burden assumed one year of exposure given 70 years of emissions, while the lifetime time-weighted lung burden as-

sumed 45 years of exposure given 70 years of emissions. These wet lung burdens were then divided through by the 70 year life expectancy to obtain a total retained wet lung burden over lifetime. Finally, the 1 year and lifetime ratios of lifetime wet lung dose and lifetime of emissions were scaled by the number (population) of workers (POP) inside of the exposure zones to define the final RiF values (eqn (11)).

$$RiF_{i,j} = \frac{EXP_{int,i,j} \cdot POP_j}{E_{life,i,j}} \quad (11)$$

The number of exposed workers was estimated from Walser *et al.* and defined as a lognormal distribution with a geometric mean of 8.7 and geometric standard deviation of 2.8 (see ESI†).[31] Three different POP scenarios were defined as low, average and high. These three scenarios represented the 5% confidence interval, geometric mean and 95%-CI of the distribution, respectively.

2.5 Dose–response relationship and effect factor for nano-TiO$_2$

The EF is interpreted from the underlying dose–response relationship of a substance.[41] The EF was estimated based on the USEtox approach,[41] defined according to eqn (12):

$$EF_i = \frac{0.5}{ED_{50,h,int,i}} \quad (12)$$

where $ED_{50,h,int,i}$ is defined as the human-equivalent (h) dose at which 50% of population experiences a carcinogenic or non-carcinogenic impact upon inhalation exposures and where 0.5 represents the fraction of the worker population that experiences the adverse human health impact.[41] Unlike

USEtox which is concerned with external exposure concentrations, the ED_{50} considered here (eqn (13)) is reported as an internal dose per g of wet lung in order to be in agreement with the RiF that is represented as a lifetime-averaged internal wet lung dose.

$$ED_{50,h,int,i} = \frac{ED_{50a,t,int,i}}{AF_a \cdot AF_t} \qquad (13)$$

$ED_{50a,t,int}$ (mg per g-wet lung) is the animal (a) internal dose (int) of nano-TiO_2 per gram of lung that results in a 50% response rate, t is the duration of the study (e.g. chronic), AF_a is an interspecies extrapolation factor (i.e. between animals to humans), and AF_t is a study-time conversion factor (i.e. between acute to chronic studies).[41,62,63] Dose–response data reported for dry lung samples were converted to wet lung with the conversion factor of 0.11 based on previous results showing that nearly 89% of the lung-weight is lost after drying.[64] Interspecies extrapolation factors account for the difference in physiology, such as breathing and body weight, between species, however a factor of one was applied in this study, under the assumption that effects based on internal doses were equivalent in animals and humans.[62] Furthermore, the $ED_{50a,t,int}$ assumed a 1:1 correlation of inflammation, reported as *extra risk*, and disease probability. Extra risk is the fraction of animals that respond to a dose, among animals who do not respond, effectively taking into account the background response rate.[65] An AF_t of 2 was used to convert sub-chronic dose–response data to chronic-equivalent values.[41,62]

$ED_{50a,t,int}$ values were defined using the benchmark dose (BMD) approach[66] and estimated using the Netherland's National Institute for Public Health and the Environment's (RIVM) PROAST software (www.rivm.nl). The BMD approach is an alternative to the no-observable-adverse-effect-level (NOAEL) or lowest-observable-adverse-effect-level (LOAEL) methods used to estimate the dose–response relationship. The BMD was estimated from its corresponding benchmark response (BMR), defined as the level of response (i.e. adverse health impact) considered significant.

Concerning the calculation of the carcinogenic EF (EF_C), there was no single carcinogenic animal study involving exposure to multiple dosing levels of nano-TiO_2. However, in 2011 the U.S. National Institute of Occupational Safety and Health (NIOSH) conducted a risk assessment using a combined set of nano-TiO_2 and fine-TiO_2 toxicological data.[67,68] Using that same dataset, a carcinogenic ED_{50} was calculated as the dose where 50% of the exposed animals developed lung tumors. Briefly, two chronic, whole-body, inhalation studies by Lee *et al.* and Muhle *et al.* looked at the tumor rates of male and female Sprague-Dawley and Fischer-344 rats that were exposed to fine (rutile) particles of TiO_2 with average mass median aerodynamic diameter (MMAD) of 1.6 um and 1.1 um, respectively.[67,69] In Lee *et al.*, there were four exposure levels of 0, 10,

50, and 250 mg m^{-3}. In Muhle *et al.*, there were two exposure levels of 0 and 5 mg m^{-3}. Heinrich *et al.* completed a chronic, whole-body, inhalation study on Wistar female rats exposed to 10 mg m^{-3} of nano-TiO_2 with average MMAD of 0.027 um.[70] The dose–response relationships of ENMs with different diameters are known to be more strongly correlated with surface area as opposed to mass-based dose metrics.[71] Therefore, the doses were converted to surface area based doses using their reported conversion factors of 4.99 m^2 g^{-1} for the fine-particulate and 48 m^2 g^{-1} nano-TiO_2. The BMR was set to 50% *extra risk* in total lung tumor development. Typically a BMR of 10% would be analogous to a corresponding NOAEL value, which would require that the resulting BMD is extrapolated to the ED_{50}.[72] Instead, the BMR was set to 50% *extra risk* and assumed to correspond directly to the ED_{50}.

For the non-carcinogenic EF (EF_{NC}), the BMR was defined as the 50% increase in lung-inflammation, according to bronchoalveolar lavage (BAL) results of rats and mice exposed to nano-TiO_2 at concentrations of 0.0 mg m^{-3} (control), 0.5 mg m^{-3}, 2.0 mg m^{-3} and 10 mg m^{-3} for 6 hours per day, 5 days per week, for 13 weeks.[73] Lung inflammation was interpreted as the percent change in neutrophil count (i.e. neutrophil counts per 200 total cellular samples) as a function of internal nano-TiO_2 lung burden.[73]

3. Results

3.1 Exposure scenarios and occupational, indoor air emissions of nano-TiO_2

Although the emission rates for ES1–ES4 were the same (6.72 × 10^2 mg min^{-1}), their total daily emissions (Table 3) were not equivalent due to changes in the frequency of the emission events.

Total daily emissions for ES1–ES3 varied by less than one-order of magnitude even though emission frequencies were noticeably different. Particularly, ES2 was characterized by 60 minute emission cycles with 60 minute pauses in-between, resulting in total daily nano-TiO_2 emissions of 1.61 × 10^5 mg. This was only 35% larger than ES1 even though emissions lasted just 10 minutes with 20 minute breaks in-between. ES3 had a constant all day emission event that resulted in a total daily nano-TiO_2 emission of 3.23 × 10^5 mg, roughly 3 times the daily emission of ES1. ES4 was characterized by a single-pulse emission event that resulted in a total maximum daily nano-TiO_2 emission of 6.72 × 10^2 mg. The total daily emissions for ES5 and ES6 were roughly 2- and 4-orders of magnitude smaller, respectively, than ES1. This was in direct correlation with their 2- and 4-orders of magnitude decrease in emission rates.

3.2 Fate and transport of airborne nano-TiO_2

The results of the fate model are reported as two different NF and FF airborne concentrations (Fig. 2) during the 8 hour workday.

ES2 and ES3 reached a maximum NF airborne concentration of 8.2 × 10^4 μg m^{-3} shortly after the work-cycles began even

Table 3 Total daily emissions, average daily and maximum near-field and far-field airborne concentrations

No.	Exposure scenario	Total daily emissions (mg)	C_{NF},[a] [mg m^{-3}]	C_{FF},[a] [mg m^{-3}]	C_{NF},[b] [mg m^{-3}]	C_{FF},[b] [mg m^{-3}]
ES1	e-high, *f-short*	1.08×10^5	6.50×10	3.45×10	2.49×10	1.48×10
ES2	e-high, *f-long*	1.61×10^5	8.15×10	5.09×10	4.07×10	2.54×10
ES3	e-high, *f-all day*	3.23×10^5	8.15×10	5.09×10	8.08×10	5.02×10
ES4	e-high, *f-single pulse*	6.72×10^2	3.63×10	6.01×10	0.170×10	0.106×10
ES5	e-medium, *f-short*	1.08×10^3	0.677×10	0.371×10	0.271×10	0.169×10
ES6	e-low, *f-short*	1.08×10	6.77×10^{-3}	3.71×10^{-3}	2.71×10^{-3}	1.69×10^{-3}

C: exposure concentration. [a] Maximum daily concentrations during work hours. [b] Average daily concentrations during the working hours.

though emissions were ongoing throughout the remainder of the workday. Maximum NF daily airborne concentrations in ES1, ES5 and ES6 reached 6.5×10^4 μg m^{-3}, 6.8×10^2 μg m^{-3} and 6.8×10 μg m^{-3}, respectively, but were still increasing at the time the work-cycle ended and emissions stopped. The maximum NF airborne concentration for ES4 of 3.6×10^4 μg m^{-3} coincided with the single pulse emission event at the beginning of the work-day. The trends in FF concentrations were similar to the NF, however these concentrations were on average 50% lower than their respective NF values.

Average daily airborne concentrations in both the NF and FF during working hours were 45% lower than their corresponding maximum daily values. However, this correlation was not linear, particularly for ES1, ES2, and ES4 (Fig. 2). While there were distinct differences in the NF and FF concentrations during the emission events, the concentration gradient quickly dissipates during non-emission events. In all cases, airborne concentrations effectively reached zero before the next work day, and thus concentrations were not cumulative from day to day (see ESI†).
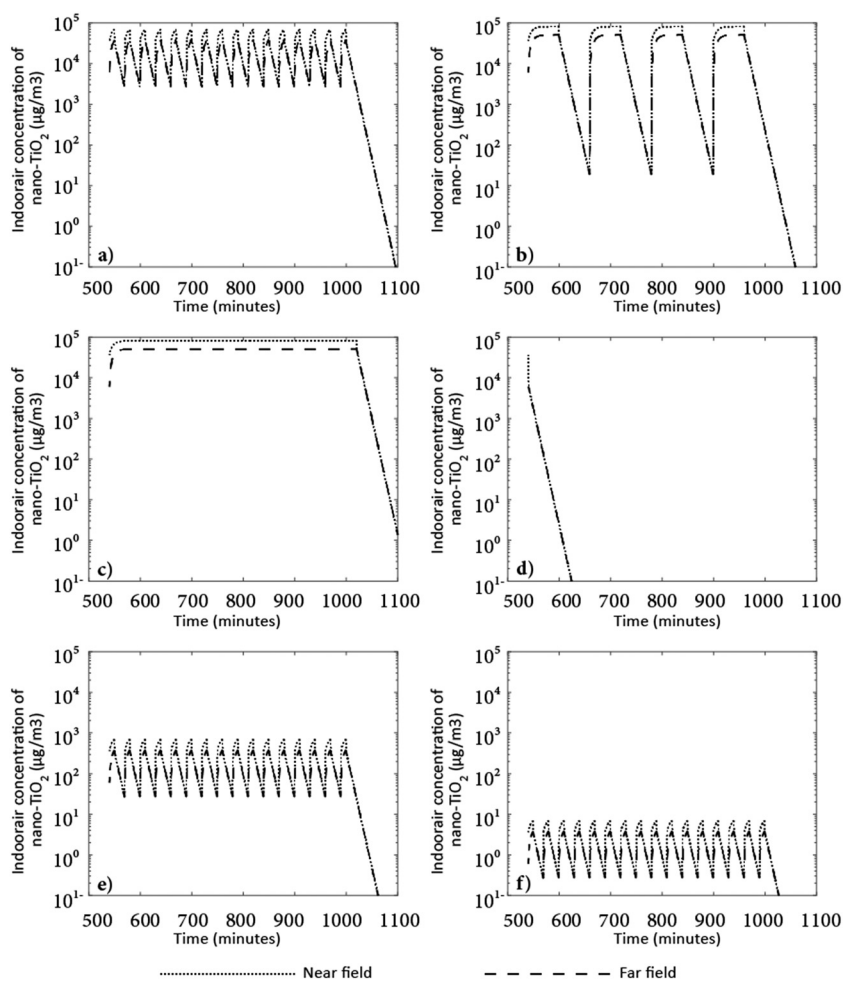

Fig. 2 Results of the fate and transport model for ES1–ES6 (a–f) showing changes in the near and far field airborne concentrations of nano-TiO$_2$ over the course of the 8 hour workday. Note that the beginning of the workday begins at minute 500 and ends just after minute 980.

The dominant mechanism driving the fate and transport of nano-TiO_2 was the air exchange between the indoor and outdoor air compartments and, to a lesser extent, the interzonal air flow between the NF and FF. In ES1, during the first minute of the first work-cycle, nearly 94% of the nano-TiO_2 remained in the indoor air (*i.e.* combined NF and FF), while 5.7% had been transferred to outside air (Fig. 3).

An additional 0.0025% of the emissions in ES1 had been transformed into larger aggregates and 0.0021% had settled to the surface due to gravitational settling. By the end of the first 10 minutes of that emission cycle, the amount of nano-TiO_2 remaining in the indoor air was only 55.84%, while 44% had been transferred to the outdoor air. The proportion of the emissions that had been removed by aggregation slightly increased to 0.0030% by the second and third minute and then fell back to 0.25% by the end of the emission event. The proportion of emissions removed by gravitational settling onto surfaces increased by over an order of magnitude to 0.03%. These trends continued through the workday whereby the exchange of indoor with outdoor air contributed to nearly 99% removal of the total daily emissions (Fig. 3). The contributions from gravitational settling and aggregation remained minimal and accounted for roughly 0.07% and 0.00005% of nano-TiO_2 removal from the indoor air. By the end of the final minute of the last emission event of the workday, just 1.0% of the total daily emissions remained in the indoor air compartment, as non-agglomerated nano-TiO_2.

The overall fate and transport patterns for ES2, ES3 and ES4 were similar to ES1, but they differed by the rates at which the indoor air concentrations of nano-TiO_2 decreased. For example, after only 40 minutes, the amount of nano-TiO_2 emissions that remained in the indoor air were 25%, 19%, 19% and 0.49% for ES1, ES2, ES3 and ES4, respectively. The relative amount of nano-TiO_2 emissions that remained in the indoor air decreased at the fastest rate for ES4 since it was only a single pulse event without further addition of nano-

TiO_2 over time during the workday. Thus, the effect of the removal mechanisms, mainly driven by the overall air exchange rate of the room, was more apparent in this scenario. Although the emission rates of ES5 and ES6 were lower than ES1, they had the same relative fate and transport pattern as ES1.

3.3 Exposure to and retained-intake fraction of occupational indoor air emissions of nano-TiO_2

The results of the MPPD model showed that 75.2% of the airborne nano-TiO_2 deposited into the lung, irrespective of the exposure scenario or concentration of particles in the air (see ESI†). The regional deposition was 9.8%, 24.6% and 40.8% in the upper airway, tracheobronchial region and the pulmonary (*i.e.* alveolar) regions, respectively. The results of the PBPK model, which estimated the clearance and ultimate retention of that deposited fraction, are reported as mass of nano-TiO_2 per mass of wet lung (Table 4).

In general, greater total emissions (Table 3) resulted in greater total lung burdens (Table 4) (*e.g.* ES1–3 *versus* ES4–6). Over the course of each work day the wet lung burden increased with all emission events. Between emissions, internal lung doses continued to rise and between workdays or workweeks (*i.e.* over the weekends) the lung burden did not decrease sufficiently to clear the lung of its total nano-TiO_2 load (Fig. 4). For example, the maximum exposure by the end of the first work-week in ES1 was 333 μg per g-wet lung, while the remaining lung burden at the beginning of the second work-week was 238 μg per g-wet lung. This trend continued until the 5th work-week, after which maximum weekly accumulations slowed considerably, having already reached 453 μg per g-wet lung which was 95% of the maximum lung burden of 478 μg per g-wet lung observed at the end of the year (Fig. 4). Similar trends were seen in the other exposure scenarios except for ES6, whose total lung burden continually
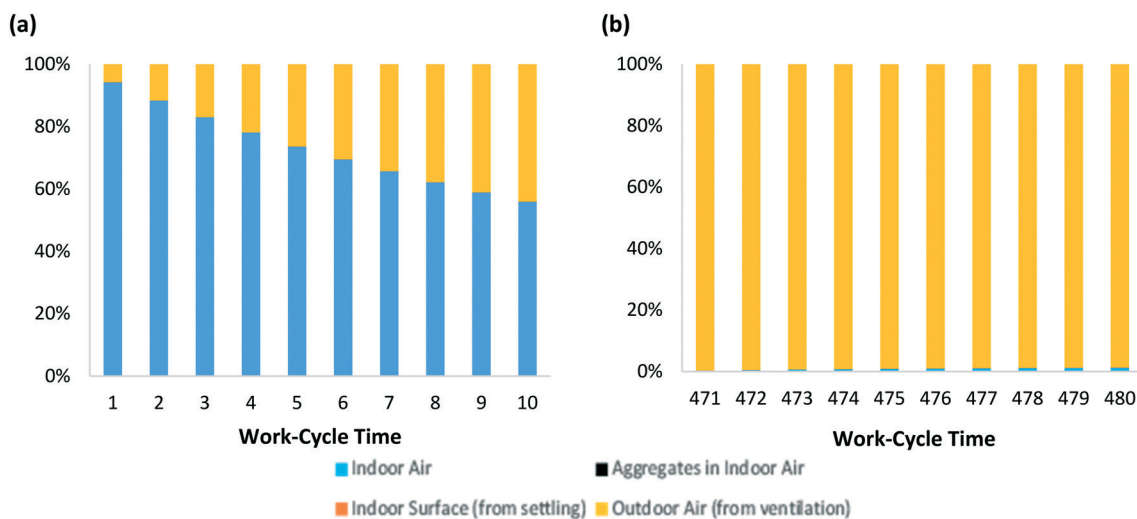

Fig. 3 Mass fraction of total nano-TiO_2 emitted in the day, per "compartment" during (a) the first 10 minutes of the first emission cycle of ES1 and (b) the final 10 minute emission cycle of ES1 at the end of the work day.

Table 4 Results for the internal wet lung burden (μg per g-wet lung) reported as either a lifetime or 1 year value

No.	Exposure scenario	Lung burden (1 year)	Lung burden (lifetime)
ES1	e-high, *f-short*	5.72×10	2.73×10^2
ES2	e-high, *f-long*	1.16×10	5.53×10^2
ES3	e-high, *f-daily*	2.50×10	1.19×10^3
ES4	e-high, *f-single pulse*	1.44×10^{-1}	7.04×10
ES5	e-medium, *f-short*	1.67×10^{-1}	8.10×10
ES6	e-low, *f-short*	1.70×10^{-2}	3.99×10

increased at a steady rate compared to the plateaus seen within a few weeks of the other ES (see ESI†).

Additionally, internal lung doses did not clear effectively between work years (*i.e.* two weeks of vacation) as was demonstrated by the 1 year time-weighted lung burden for ES1 of 5.72 μg per g-wet lung while the lifetime lung-burden was 273 μg per g-wet lung. The 1 year time weighted lung burdens ranged from a high of 25 μg per g-wet lung for ES3 to a low of 0.017 μg per g-wet lung for ES6 (Table 4). Similarly, the lifetime weighted lung burdens ranged from a high of 119 μg per g-wet lung for ES3 to a low of 4.0 μg per g-wet lung for ES6 (Table 4).

For ES1, total lung burden was mainly due to the retention of nano-TiO_2 in the interstitial tissue, where it represented up to 80% of the total retained wet lung mass by the end of

the first work-year (Fig. 5). In contrast, the pulmonary region had cleared itself of all deposited nano-TiO_2 by the beginning of each subsequent work-week. Even so, the pulmonary region contributed up to 17% of the total *maximum* retention observed each day by the end of the first work-year. The PCs located in the interstitial and pulmonary regions reached maximum retentions of 3202 μg and 4644 μg, respectively, very quickly within the first workday and did not accumulate more over the duration of the remaining exposure period. This represented roughly 0.7% and 1.0% of the total lung burden by the end of the work year. The trachea–bronchial or upper airway regions were not defined as part of the wet lung and thus do not directly contribute to the overall lung burden under consideration (see ESI†).

The physiologic pattern of retention was very similar for ES1–3, whose total yearly emissions and retained lung burdens were much greater than ES4–6. As total yearly emissions, and thus lung burdens, decreased, the pattern of retention shifted towards greater number of particles captured by the pulmonary and interstitial PCs. Subsequently, in the scenario with the lowest emissions and lowest lung burden, ES6, nearly 100% of the particles were captured by pulmonary-PCs.

As a ratio of the lung burden to total emissions, the corresponding 1 year RiF values range from a high of 7.81×10^{-10} for ES6 to a low of 2.62×10^{-11} for ES1. Similarly, the lifetime
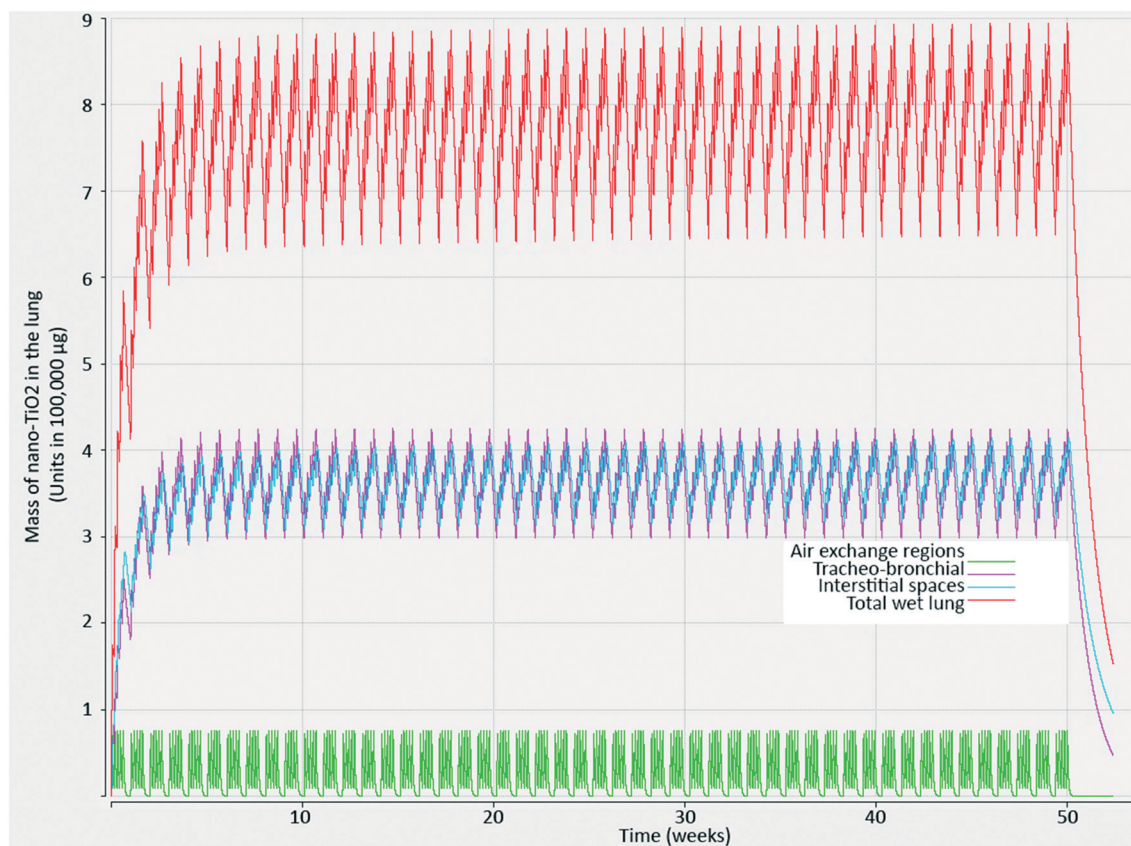

Fig. 4 Retention of nano-TiO_2 in the lung estimated over 1 full work year for ES1, whereby work continued 5 days a week (*i.e.* no work on the weekends) for 50 weeks with a 2 week holiday at the end of the year during weeks 51 and 52.
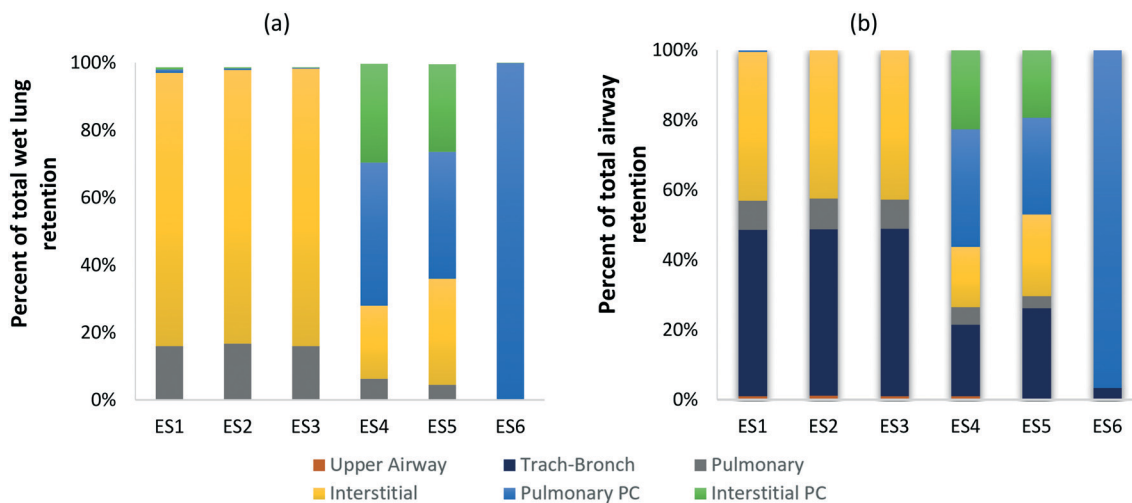
Fig. 5 Relative retention of nano-TiO$_2$ in the (a) wet lung and (b) total airway system per region of the lung, for each of the six exposure scenarios. Results represent the relative retention for the maximum exposure obtained after 1 year of work.

RiF values ranged from a high of 2.21×10^{-7} for ES6 to a low of 1.25×10^{-9} for ES1. Consequently, an inverse relationship was seen between the total yearly emissions and the RiF (Fig. 6).

As expected, the RiF increases linearly with the increasing number of workers. Thus, the RiF for the highest worker population was 1.5-orders of magnitude greater than the RiF in the lowest worker population scenario. These results corresponded directly to the 1.5-order of magnitude difference in their respective worker populations.

3.4 Dose–response relationship and effect factor for nano-TiO$_2$

The carcinogenic dose–response analysis is shown in Fig. 7. The corresponding ED$_{50,a}$ (*i.e.* BMD) was 1.43 m^2 per g-dry lung based on the excess risk of 50% over background cancer rates, with the dose being explicitly expressed as the TiO$_2$ surface area concentration per gram of dry lung. After conversion to a mass-based dose-metric, assuming a value of 48 m^2 per g-TiO$_2$, the ED$_{50,a}$ was 2.98×10^4 μg per g-dry lung. After converting the dry lung doses to wet lung, the ED$_{50,a}$ became 3.16×10^3 μg per g-wet lung. Applying the relevant extrapolation factors (eqn (13)), the resulting ED$_{50h}$ value was 1.58×10^3 μg TiO$_2$ (per g-wet lung) and the final EF$_C$ was 3.17×10^{-4} cases per μg nano-TiO$_2$ (per g-wet lung).

The results of the non-carcinogenic dose–response analysis are shown in (Fig. 8). BMD values were interpreted from the results of a sub-chronic whole-body inhalation study measuring the changes in BAL fluids upon exposure to nano-TiO$_2$. The reported benchmark doses were 27 352 μg per g-dry lung for mice and 7807 μg per g-dry lung for rats based on
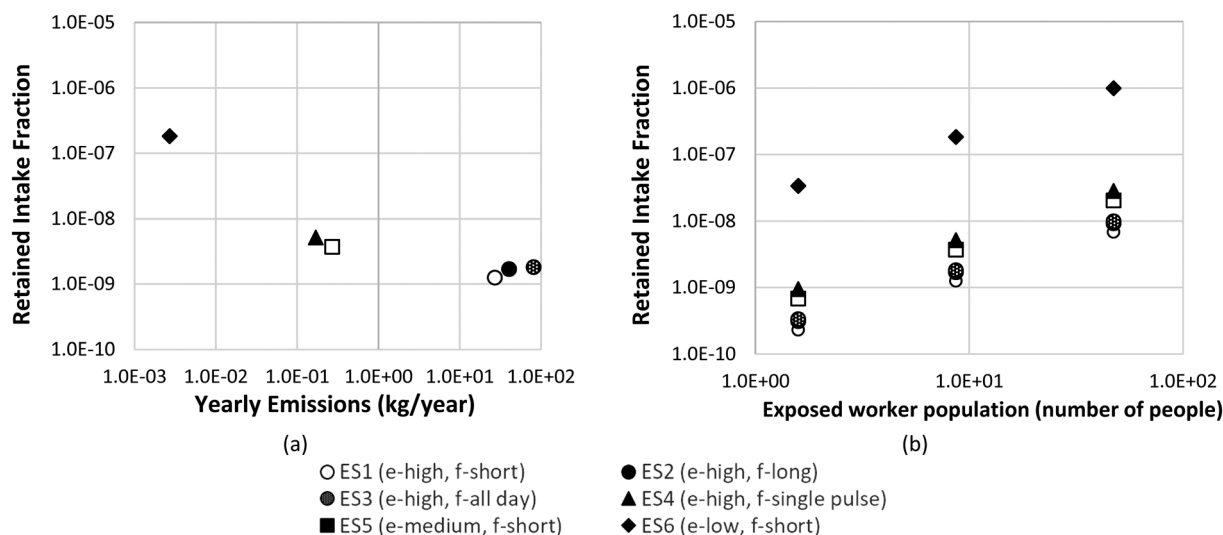

Fig. 6 Lifetime retained intake fractions as a function of (a) total yearly emissions and (b) worker population size. All axes are shown in log-scale.
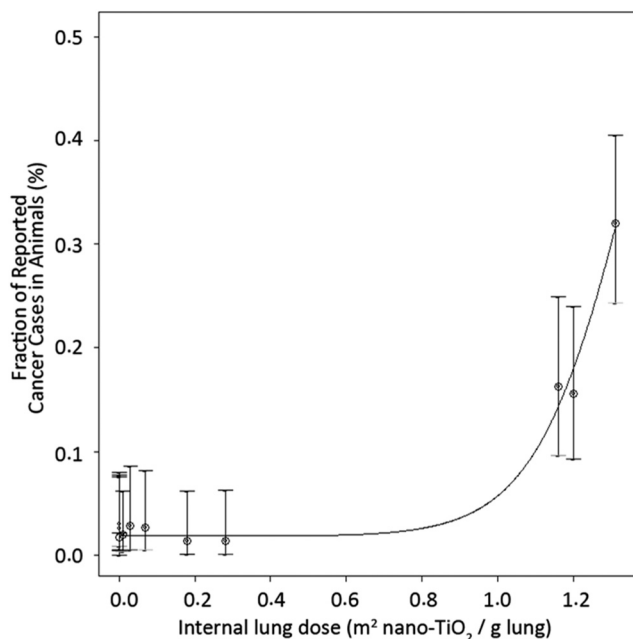
Fig. 7 Benchmark dose results for cancerous impacts in rats upon inhalation of nano-TiO$_2$ and reported as fraction of cancer cases per internal lung dose.

the excess risk of 50% over background inflammation rates. Covariation, based on species type, showed that there were distinct dose–response slopes for both mice and rats, with rats having lower BMD values (*i.e.* more sensitive). Based on the approach put forth in USEtox,[41] the BMD for rats was used to estimate the EF because it was the most sensitive species. This ED$_{50,a}$ was 8.27×10^2 μg per g-wet lung. The resulting ED$_{50,h}$ value was 4.14×10^2 μg TiO$_2$ (per g-wet lung)

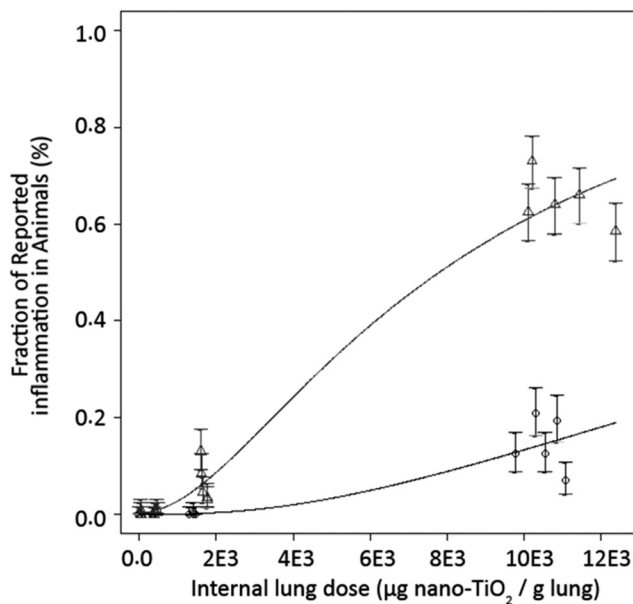**Fig. 8** Benchmark dose results for non-cancerous impacts to both mice (circles) and rats (triangles).

and the final EF$_{NC}$ was 1.21×10^{-3} cases per μg (internal) TiO$_2$ dose.

3.5 Characterization factors for human health impacts from occupational, indoor air emissions of nano-TiO$_2$

For each exposure scenario, a 1 year and lifetime CF are reported for nano-TiO$_2$ occupational, airborne emissions (Table 5). One-year CF$_C$ values ranged from a low of 3.96×10^{-4} cases of cancer per kg of nano-TiO$_2$ emissions in ES1 to a high of 5.80×10^{-2} cases of cancer per kg of nano-TiO$_2$ emissions in ES6. The 1 year, *non-carcinogenic* CF values were slightly larger and ranged from a low of 1.51×10^{-3} cases of lung inflammation per kg of nano-TiO$_2$ emissions to a high of 2.21×10^{-1} cases of lung inflammation per kg of nano-TiO$_2$ emissions. Compared to 1 year exposure periods, lifetime CF values were generally 1–2 orders of magnitude larger.

Whereas the differences between the 1 year and lifetime CF were between 1–2 orders of magnitude, the differences between the average worker population and the low or high populations was less than an order of magnitude for ES1–ES6. Lower working populations resulted in slightly higher RiF values but greater CF, while higher working populations resulted in lower RiF values but lower CF.

An inverse relationship is then noticed between the total emissions and the corresponding CF (see ESI†). Consequently, ES6 had the largest CF$_C$ and CF$_{NC}$ values even though it had the lowest total yearly emissions, while ES1–3 had the lowest CF values but the largest emissions.

4. Discussion

Currently, the estimation of ENM emissions, fate, exposure and human health impacts from indoor air exposure within LCA have been largely un-addressed in the scientific literature. Steady-state fate and exposure methodologies[12–16] provide a straightforward first approximation of ENM behavior in the environment, while dynamic models may provide additional insight are not captured by steady-state models. However, dynamic models require more data such as reported or estimated emissions over time. In this paper, a dynamic model was utilized for estimating indoor airborne emissions of nano-TiO$_2$, a spherical, metal oxide ENM powders. Hence, this approach may have limited application for estimating the effects of producing or handling ENMs whose physical characteristics are not spherical or are in solution (*i.e.* whose emissions are directly to soil and/or water).

The difference between steady-state and dynamic models and their results was apparent in this study. For example, if a steady-state approximation is applied (see ESI†)[45] to ES1, the resulting NF airborne concentration would be 3.52 mg m^{-3}. This result is approximately 95% smaller than the maximum NF concentration predicted by the dynamic model, which demonstrated increases in nano-TiO$_2$ concentration over the course of subsequent emissions. In the dynamic model, removal by aggregation and gravitational settling was minimal,

Table 5 Effect factors (EF), retained-intake fractions (RiF), carcinogenic characterization factors (CF_C) and non-carcinogenic characterization factors (CF_{NC}) for the six emission and exposure scenarios, worker population, as well as timeframe of the exposure

Reference	EF_C	EF_{NC}	1 year[a] RiF	1 year[a] CF_C	1 year[a] CF_{NC}	Lifetime[a] RiF	Lifetime[a] CF_C	Lifetime[a] CF_{NC}	Low population[b] RiF	Low population[b] CF_C	Low population[b] CF_{NC}	High population[b] RiF	High population[b] CF_C	High population[b] CF_{NC}
(Units)	cases per kg TiO_2 (intake)[c]		kg TiO_2 (intake)[c] per kg TiO_2 (emitted)	cases per kg TiO_2 (emitted)		kg TiO_2 (intake)[c] per kg TiO_2 (emitted)	cases per kg TiO_2 (emitted)		kg TiO_2 (intake)[c] per kg TiO_2 (emitted)	cases per kg TiO_2 (emitted)		kg TiO_2 (intake)[c] per kg TiO_2 (emitted)	cases per kg TiO_2 (emitted)	
ES1 (e-high, f-short)	3.17×10^5	1.21×10^6	2.62×10^{-11}	8.31×10^{-6}	3.17×10^{-5}	1.25×10^{-9}	3.96×10^{-4}	1.51×10^{-3}	2.29×10^{-10}	7.25×10^{-5}	2.77×10^{-4}	6.83×10^{-9}	2.16×10^{-3}	8.25×10^{-3}
ES2 (e-high, f-long)			3.55×10^{-11}	1.12×10^{-5}	4.29×10^{-5}	1.69×10^{-9}	5.35×10^{-4}	2.04×10^{-3}	3.09×10^{-10}	9.79×10^{-5}	3.74×10^{-4}	9.22×10^{-9}	2.92×10^{-3}	1.11×10^{-2}
ES3 (e-high, f-all day)			3.82×10^{-11}	1.21×10^{-5}	4.62×10^{-5}	1.82×10^{-9}	5.75×10^{-4}	2.19×10^{-3}	3.33×10^{-10}	1.05×10^{-4}	4.02×10^{-4}	9.92×10^{-9}	3.14×10^{-3}	1.20×10^{-2}
ES4 (e-high, f-single pulse)			1.05×10^{-11}	3.34×10^{-5}	1.27×10^{-4}	5.16×10^{-9}	1.63×10^{-3}	6.24×10^{-3}	9.46×10^{-10}	2.99×10^{-4}	1.14×10^{-3}	2.82×10^{-8}	8.92×10^{-3}	3.40×10^{-2}
ES5 (e-medium, f-short)			7.64×10^{-11}	2.42×10^{-5}	9.23×10^{-5}	3.71×10^{-9}	1.18×10^{-3}	4.48×10^{-3}	6.80×10^{-10}	2.15×10^{-4}	8.21×10^{-4}	2.03×10^{-8}	6.42×10^{-3}	2.45×10^{-2}
ES6 (e-low, f-short)			7.81×10^{-10}	2.47×10^{-4}	9.44×10^{-4}	1.83×10^{-7}	5.80×10^{-2}	2.21×10	3.36×10^{-8}	1.06×10^{-2}	4.05×10^{-2}	1.00×10^{-6}	3.17×10^{-1}	1.21×10
Reference (Units)	EF_C cases per kg TiO_2 (intake)[d]	EF_{NC}	iF kg TiO_2 (intake)[d] per kg TiO_2 (emitted)	CF_C cases per kg TiO_2 (emitted)	CF_{NC}	iF kg TiO_2 (intake)[d] per kg TiO_2 (emitted)	CF_C cases per kg TiO_2 (emitted)	CF_{NC}	RiF	CF_C	CF_{NC}	RiF	CF_C	CF_{NC}
Pini et al.	1.21×10^2	4.98×10^{-3}	—	—	—	1.18×10^{-4}	1.43×10^{-2e}	5.85×10^{-7}	—	—	—	—	—	—
Ettrup et al.	4.46×10^{-2}	3.33×10^{-1}	—	—	—	4.25×10^{-5}	1.90×10^{-6}	1.70×10^{-5}	—	—	—	—	—	—
USEtox	—	—	1.19×10^{-4f}	—	—	—	—	—	—	—	—	—	—	—

[a] Reported for the average number of workers. [b] Reported for the lifetime exposure scenarios. [c] Intake reported as kg TiO_2 per g-lung. [d] Intake converted from kg TiO_2 per kg-bw in the original publications to kg TiO_2 per g-lung in this current study. [e] Reported as an ED4: 4% increase in inflammation rate. [f] Reported for generic 'organics' and 'inorganics' and not specific for nanoparticles or titanium dioxide.

which might be expected given that the settling velocity of even 1 um sized particles is *circa* 12.5 cm h^{-1}.[48] These removal mechanisms will likely become more important if air exchange rates are kept low.[74,75]

The exposure model used in this paper departed from conventional LCIA methods that assume inhalation exposures are linearly related to an individual's respiration rate. Walser *et al.*[31] recently proposed, and Pini *et al.*[15] estimated, final retention values based on steady-state deposition and clearance using the MPPD model. The reported lifetime RiFs in the current study were between 2- to 5-orders of magnitude less than what was reported in Pini *et al.* However, the total mass of retained nano-TiO$_2$ estimated in the current paper was similar to those from previously reported *in vivo* studies which were on the order of hundreds of days in the air exchange and interstitial regions of the lung.[30,60,76] Thus, it may seem that the inhalation of nano-TiO$_2$ and other similar metal oxide ENMs may be particularly overestimated with the use of steady-state models. Of the three main pathways in the PBPK model that governed ENM retention in the lung, translocation of loaded-PCs from the pulmonary (*i.e.* alveolar) to the tracheobronchial region was the limiting factor determining clearance of nano-TiO$_2$ from the lung. This value was modified to reflect the slower clearance rate of particulates in the human lung compared with the rat lung.[60] In the highest exposure scenario, PCs were easily saturated and overburdened, leading to accumulation in many of the lung regions. The unlimited accumulation found in the air-exchange and interstitial regions for some of the exposure scenarios may be occurring due to mucociliary clearance becoming overburdened, which cannot remove particles at a fast-enough rate to reach zero lung burden even at times of low- or no-exposure. However, these results may also be limited by the model's capability to adjust for the increase or decrease of mucociliary clearance activity depending on the mass loading of ENM in the airway. The current version of the PBPK model uses a constant transfer factor to describe this mechanism instead of one that might change based on the internal load. Additionally, the high concentration of nano-TiO$_2$ found in the tracheobronchial region was expected given the primary particle sizes upon exposure were assumed to be 21 nm. Particles ≤100 nm have a greater chance of reaching the alveolar region, however particles ≤30 nm, particularly those below 10 nm,[60] will show greater deposition and retention in the tracheobronchial region due to airflow dynamics of smaller diameter particles.[30]

The RiF defined in this study showed an inverse relationship between the amount of nano-TiO$_2$ emitted into the occupational indoor air workplace and the retained amount of nano-TiO$_2$ in the lung. This finding is counter-intuitive given that iF values in conventional LCIA methods are independent of the emission rates or total emission amounts. The inverse relationship can be explained by the saturation of PCs in the lungs and the relative contribution of PC-sequestered ENM to the overall wet lung burden. Neither of these scales linearly with emission rate, thus bearing the inverse relationship dis-

covered in this study. As shown in the results for the exposure, after saturation, the relative contribution of PCs loaded with nano-TiO$_2$ to the overall wet lung burden decreases as emission rates increases. The amounts in the pulmonary region and interstitium of the lungs scale proportionally with the emission rate after the PCs are saturated. The lifetime RiF, for example, differed by a maximum two-orders of magnitude while emissions per year increased up to four-orders of magnitude. This is because PCs still play a major role at lower emission rates. This highlights the importance of the emission rate on the RiF when considering the target organ's physiology.

The RiF and exposure results should be interpreted with caution. Although adaptations were made to an original animal-based exposure model[28] to estimate bio-distribution in humans, the results of this model have not been validated by experimental evidence. In addition, the original PBPK model published by Li *et al.*[28] was built based on exposure concentrations that were 2-orders of magnitude lower than the highest exposure scenario presented in this study, which is in effect the worst-case scenario. The results of applying the PBPK-rat model to human exposure scenarios should be considered as potential impacts as opposed to absolute values. The resulting RiF calculated in this paper also did not include the effects and use of PPE in the work environment. At the time of this study, it was not evident which occupational scenarios would require PPE, at what rate PPE would be used and the effectiveness of the PPE to filtering ENM. However, it is expected that some level of PPE would apply, resulting in lower amounts of exposure than predicted in this paper. Therefore, if patterns of PPE usage are known, this should be included in the exposure estimation.

The RiF was also significantly influenced by the exposure timeframe assumed in the model, whereby 1 year RiF and their corresponding CF were one- to two-orders of magnitude smaller than their lifetime counterparts. The relative decrease in retained-intake and, therefore, cases of human health impact per emitted mass of nano-TiO$_2$ was expected given the significantly shorter amount of exposure time in the 1 year exposure scenarios. In this way, the CF can be used in a manner that is compatible with LCIA methodologies that contain different "perspectives" based on decision maker's preferences for short-term *versus* long-term priorities and objectives.[25,77]

Additionally, the CF presented in this study were calculated for inhalation exposures in the occupational setting, since inhalation of dusts and powders is the primary intake route in the workplace scenario.[31] While the fate and transport model predicts indoor surface concentrations that could be used for approximating dermal exposures, dermal exposure and thus toxicity is expected to be low unless in contact with broken skin.[78–82] Furthermore, apart from direct impacts to the lungs and lung-related injuries, ENMs that are deposited in the lung may translocate to other regions of the body after inhalation.[83–85] Although the exposure model presented in this approach allows for the estimation of ENMs

in 10 other organs of the body, these values were not yet used to address systemic-human health impacts upon inhalation to nano-TiO$_2$. Future work in this area should address the compounded effects from multi-system organ toxicity upon inhalation to ENMs.

The EF$_C$ reported in this study was almost 1-order of magnitude smaller than the EF$_{NC}$. It should be noted that the non-carcinogenic endpoint was pulmonary inflammation, a precursor to the carcinogenic endpoint of pulmonary tumors. Thus, these results intuitively make sense. It would be expected that many more cases of a non-cancerous diseases occur compared with more advanced pathologies such as cancer. This is supported by Ettrup *et al.* who similarly report an EF$_C$ value of 1.54×10 cases per kg TiO$_2$ (intake) that is under 1-order of magnitude lower in value than their reported EF$_{NC}$ of 1.15 cases per kg TiO$_2$ (intake).[16] However, Pini *et al.* report an EF$_C$ of 4.19×10^2 cases per kg TiO$_2$ (intake) that is 4-orders of magnitude greater than their reported EF$_{NC}$ of 1.72×10^{-2} cases per kg TiO$_2$ (intake), thus implying that there are many more expected cases of cancer compared with inflammation.[15] A likely explanation regarding this discrepancy is the fact that Pini *et al.* used an inflammation study[73] as a proxy for the carcinogenic endpoint.[15] Therefore, a comparison of their EF$_C$ to the EF$_{NC}$ in this current paper as well as Ettrup *et al.* is more appropriate. After correcting for intake per lung weight to intake per body weight, the EF$_{NC}$ reported in the current paper was 4-orders of magnitude larger than Pini *et al.*'s (EF$_C$) and over 6-orders of magnitude larger than Ettrup *et al.*'s. Similarly, the EF$_C$ reported in the current paper is over 6-orders of magnitude greater than Ettrup *et al.*'s and no comparison is made to Pini *et al.*'s value for the aforementioned reasons.

While the current study utilized the BMD approach to estimate the ED$_{50}$ values, Ettrup *et al.* and Pini *et al.* extrapolated from NOAEL values. N(L)OAELs are known to ignore the shape of a dose–response curve, meaning that the value may not actually reflect a dose at which *no* or *the lowest* effect occurs.[65,66,86–89] The magnitude of these indicators also unintuitively decrease (*i.e.* become less conservative) as the certainty of a study increases. For example, studies with more animals compared with ones with less animals per dosing group have greater chances of showing a statistically significant difference in the response rate *versus* the control. Although the study with less animals per dosing group will have a lower chance of showing statistical significance between the dosing and control groups, leading to the establishment of an NOAEL.[65] Furthermore, in the current study, the ED$_{50}$ values for both the cancerous and non-cancerous endpoint were interpreted from toxicological data that did not report a 50% response rate. This extrapolation in turn adds to the uncertainty of the estimated EF. Thus, the influence of the EF on the resulting value of the CF may overshadow the influence and differences between steady-state and dynamic fate and exposure modeling.

Ultimately, the lifetime CF$_C$ and CF$_{NC}$ values reported in this paper were on the order of 2- to 3-orders of magnitude greater than Ettrup *et al.* or Pini *et al.*, except for ES6's CF which had a greater CF$_{NC}$ value compared with Pini *et al.*'s CF$_C$ (which was estimated for a non-carcinogenic endpoint as explained above). Due to the limited purposeful and limited exposure in the 1 year CF calculations, the CF$_C$ and CF$_{NC}$ in the current study were further reduced resulting in values that were within 1-order of magnitude of Ettrup *et al.* However, their underlying factors (*i.e.* EF, iF, RiF) values were extremely different and thus the overlapping CF results are more coincidental than correlated.

5. Conclusion

A dynamic LCIA model was presented for calculating the human health impacts resulting from the exposures to occupational, airborne emissions of nano-TiO$_2$. The results demonstrate how such models can be used to estimate the fate of and exposure to certain ENMs within LCA studies. In the context of conventional, steady-state models, ENMs are not thought to attain thermodynamic equilibrium in their local mediums, invalidating the use of equilibrium partition coefficients to describe their fate and exposure in the environment.[23] Instead, kinetic models are better equipped to estimate the concentration-dependent behavior of ENMs in the environment. Furthermore, occupational indoor airborne ENM emissions are likely to be episodic and vary over time. Accordingly, the results of this study depart from the results of previous steady-state models presented in the literature.[15,16] Between the dynamic and steady-state models, the differences in the estimated airborne concentrations of nano-TiO$_2$ were roughly 1-order of magnitude. Such modest differences are reasonable given that the fate and transport of nano-TiO$_2$ was shown to be governed mainly by advection as opposed to other ENM-specific behaviors and transformations. However, the estimated intake (*i.e.* RiF, iF) of the current study were many orders of magnitude smaller than those of the steady-state models reported by Pini *et al.* and Ettrup *et al.*[15,16] The total lung burden in the current study was similar to previously published estimates in animal studies,[30,60,76] and thus indicate that steady-state models are overestimating the deposition and final retention of nano-TiO$_2$ in the lungs. Additionally, the model demonstrated that the fraction of nano-TiO$_2$ that is deposited and retained in the lung is dependent on the originating emission magnitude and thus airborne concentration in the workplace. This leads to a non-constant, and more precisely, non-linear RiF that is counter to conventional LCIA modeling.

In general, life cycle inventories are temporally and spatially undefined, leaving a disconnect between how to apply dynamic models to current life cycle data. If there is exact information regarding the rate of production for the reference-flow (*i.e.* product), then the reported emissions for that reference-flow could be defined as an emission rate for use in the fate and transport model. Often, this level of life cycle inventory detail might not be available. Case-by-case CF modeling and LCA studies are also likely to be time

consuming and limited based on the availability of other site-specific data needed in the model. Instead, researchers in the field of LCA might profit from creating context-dependent emission scenarios and fate and exposure models such as was presented in this paper. This could result in the creation of a handful of CFs per substance-scenario that satisfy an average and expected range of inventories for that emission flow. Future models should create classes of different CF based on parameters in the models such as air exchange rates, room volume, as well as the ENM size[16] and species that may influence their fate, exposure and toxicity. Even with limited insight into the types of ENM emissions in a practitioner's inventory, they might be able to more appropriately choose from one of these CF classes.

Acknowledgements

References

1 M. E. Vance, T. Kuiken, E. P. Vejerano, S. P. McGinnis, M. F. Hochella, D. Rejeski and M. S. Hull, *Beilstein J. Nanotechnol.*, 2015, **6**, 1769–1780.

2 R. A. Yokel and R. C. MacPhail, *J. Occup. Med. Toxicol.*, 2011, **6**, 7.

3 V. Stone, *Engineered Nanoparticles: Review of Health and Environmental Safety*, 2009.

4 M. Greßler and S. Nentwich, *Nano Trust Dossiers*, 2012, vol. 27, pp. 1–6.

5 A. A. Keller, S. McFerran, A. Lazareva and S. Suh, *J. Nanopart. Res.*, 2013, **15**, 1–17.

6 F. Gottschalk and B. Nowack, *J. Environ. Monit.*, 2011, **13**, 1145.

7 T. Y. Sun, F. Gottschalk, K. Hungerbühler and B. Nowack, *Environ. Pollut.*, 2014, **185**, 69–76.

8 F. Gottschalk, T. Sun and B. Nowack, *Environ. Pollut.*, 2013, **181**, 287–300.

9 F. Gottschalk, T. Sonderer, R. W. Scholz and B. Nowack, *Environ. Sci. Technol.*, 2009, **43**, 9216–9222.

10 A. A. Keller, W. Vosti, H. Wang and A. Lazareva, *J. Nanopart. Res.*, 2014, **16**, 2489.

11 S. Gavankar, S. Suh and A. F. Keller, *Int. J. Life Cycle Assess.*, 2012, **17**, 295–303.

12 M. J. Eckelman, M. S. Mauter, J. A. Isaacs and M. Elimelech, *Environ. Sci. Technol.*, 2012, **46**, 2902–2910.

13 B. Salieri, S. Righi, A. Pasteris and S. I. Olsen, *Sci. Total Environ.*, 2015, **505**, 494–502.

14 M. Miseljic and S. I. Olsen, *J. Nanopart. Res.*, 2014, **16**, 1–33.

15 M. Pini, B. Salieri, A. M. Ferrari, B. Nowack and R. Hischier, *Int. J. Life Cycle Assess.*, 2016, **21**, 1452–1462.

16 K. Ettrup, A. Kounina, S. F. Hansen, J. A. J. Meesters, E. B. Vea and A. Laurent, *Environ. Sci. Technol.*, 2017, **51**, 4027–4037.

17 R. Hischier and T. Walser, *Sci. Total Environ.*, 2012, **425**, 271–282.

18 S. Hellweg, E. Demou, M. Scheringer, T. E. McKone and K. Hungerbühler, *Environ. Sci. Technol.*, 2005, **39**, 7741–7748.

19 A. Meijer, M. Huijbregts and L. Reijnders, *Int. J. Life Cycle Assess.*, 2005, **10**, 309–316.

20 S. Hellweg, E. Demou, R. Bruzzi, A. Meijer, R. K. Rosenbaum, M. A. J. Huijbregts and T. E. McKone, *Environ. Sci. Technol.*, 2009, **43**, 1670–1679.

21 T. Walser, R. Juraske, E. Demou and S. Hellweg, *Environ. Sci. Technol.*, 2014, **48**, 689–697.

22 E. Kikuchi, Y. Kikuchi and M. Hirao, *Ann. Occup. Hyg.*, 2012, **56**, 829–842.

23 A. Praetorius, N. Tufenkji, K.-U. Goss, M. Scheringer, F. von der Kammer and M. Elimelech, *Environ. Sci.: Nano*, 2014, **1**, 317.

24 R. K. Rosenbaum, T. M. Bachmann, L. S. Gold, M. A. J. Huijbregts, O. Jolliet, R. Juraske, A. Koehler, H. F. Larsen, M. MacLeod, M. Margni, T. E. McKone, J. Payet, M. Schuhmacher, D. van de Meent and M. Z. Hauschild, *Int. J. Life Cycle Assess.*, 2008, **13**, 532–546.

25 M. Goedkoop, R. Heijungs, M. Huijbregts, A. De Schryver, J. Struijs and R. Van Zelm, *Louvain Med.*, 2008, 2008.

26 J. T. K. Quik, J. A. Vonk, S. F. Hansen, A. Baun and D. Van De Meent, *Environ. Int.*, 2011, **37**, 1068–1077.

27 J. A. J. Meesters, A. A. Koelmans, J. T. K. Quik, A. J. Hendriks and D. van de Meent, *Environ. Sci. Technol.*, 2014, **48**, 5726–5736.

28 D. Li, M. Morishita, J. G. Wagner, M. Fatouraie, M. Wooldridge, W. E. Eagle, J. Barres, U. Carlander, C. Emond and O. Jolliet, *Part. Fibre Toxicol.*, 2015, **13**, 45.

29 N. Hodas, M. Loh, H.-M. Shin, D. Li, D. Bennett, T. E. McKone, O. Jolliet, C. J. Weschler, M. Jantunen, P. Lioy and P. Fantke, *Indoor Air*, 2015, **26**, 836–856.

30 H. M. Braakhuis, M. V. Park, I. Gosens, W. H. De Jong and F. R. Cassee, *Part. Fibre Toxicol.*, 2014, **11**, 18.

31 T. Walser, D. Meyer, W. Fransman, H. Buist, E. Kuijpers and D. Brouwer, *J. Nanopart. Res.*, 2015, **17**, 1–18.

32 H. H. Liu and Y. Cohen, *Environ. Sci. Technol.*, 2014, **48**, 3281–3292.

33 K. L. Garner, S. Suh and A. A. Keller, *Environ. Sci. Technol.*, 2017, **51**, 5541–5551.

34 A. G. Agrios and P. Pichat, *J. Appl. Electrochem.*, 2005, **35**, 655–663.

35 X. Chen and S. S. Mao, *Chem. Rev.*, 2007, **107**, 2891–2959.

36 P. M. Hext, J. A. Tomenson and P. Thompson, *Ann. Occup. Hyg.*, 2005, **49**, 461–472.

37 K. E. Varner, K. Rindfusz, A. Gaglione and E. Viveiros, *Nano Titanium Dioxide Environmental Matters: State of the Science Literature Review*, Washington, D.C., 2010.

38 U.S. Geological Survey, *2012 Minerals Yearbook – Titanium*, Washington, D.C., 2012.

39 R. K. Rosenbaum, A. Meijer, E. Demou, S. Hellweg, O. Jolliet, N. L. Lam, M. Margni and T. E. McKone, *Environ. Sci. Technol.*, 2015, **49**, 12823–12831.

40 Y. Wenger, D. Li and O. Jolliet, *Int. J. Life Cycle Assess.*, 2012, **17**, 919–931.

41 R. K. Rosenbaum, T. M. Bachmann, L. S. Gold, M. A. J. Huijbregts, O. Jolliet, R. Juraske, A. Koehler, H. F. Larsen, M. MacLeod, M. Margni, T. E. McKone, J. Payet, M. Schuhmacher, D. van de Meent and M. Z. Hauschild, *Int. J. Life Cycle Assess.*, 2008, **13**, 532–546.

42 M. P. Tsang, D. Hristozov, A. Zabeo, A. J. Koivisto, A. C. Ø. Jensen, K. A. Jensen, C. Pang, A. Marcomini and G. Sonnemann, *Nanotoxicology*, 2017, **11**, 558–568.

43 D. Hristozov, A. Zabeo, K. Alstrup Jensen, S. Gottardo, P. Isigonis, L. Maccalman, A. Critto and A. Marcomini, *NANO*, 2016, 1–14.

44 G. Ramachandran, *Occupational Exposure Assessment for Air Contaminants*, CRC Press, Boca Raton, 2005.

45 M. Nicas, *Am. Ind. Hyg. Assoc. J.*, 1996, **57**, 542–550.

46 E. Demou, S. Hellweg, M. P. Wilson, S. K. Hammond and T. E. McKone, *Environ. Sci. Technol.*, 2009, **43**, 5804–5810.

47 E. J. Furtaw Jr, M. D. Pandian, D. R. Nelson and J. V. Behar, *J. Air Waste Manage. Assoc.*, 1996, **46**, 861–868.

48 R. F. Phalen and R. N. Phalen, *Introduction to Air Pollution Science*, Jones and Bartlett Learning, Burlington, 1st edn, 2011.

49 M. D. Allen and O. G. Raabe, *Aerosol Sci. Technol.*, 1985, **4**, 269–286.

50 C. Kleinstreuer, Z. Zhang and Z. Li, *Respir. Physiol. Neurobiol.*, 2008, **163**, 128–138.

51 P. E. J. BALDWIN and A. D. MAYNARD, *Ann. Occup. Hyg.*, 1998, **42**, 303–313.

52 R. Clift, J. R. Grace and M. E. Weber, *Bubbles, Drops, and Particles*, Academic Press, New York, 1978.

53 U. Carlander, D. Li, O. Jolliet, C. Emond and G. Johanson, *Int. J. Nanomed.*, 2016, 625.

54 D. K. Molina and V. J. M. DiMaio, *Am. J. Forensic Med. Pathol.*, 2012, **33**, 368–372.

55 D. K. Molina and V. J. M. DiMaio, *Am. J. Forensic Med. Pathol.*, 2012, **33**, 362–367.

56 S. Fox, *Human Physiology*, McGraw-Hill, New York, 12th edn, 2010.

57 A.-M. Salmasi and A. S. Iskandrian, *Cardiac Output and Regional Flow in Health and Disease*, Springer, Netherlands, Dordrecht, 1993, vol. 138.

58 R. P. Brown, M. D. Delp, S. L. Lindstedt, L. R. Rhomberg and R. P. Beliles, *Toxicol. Ind. Health*, 1997, **13**, 407–484.

59 C. for H. R. (CII) and the N. N. I. for P. H. and the E. (RIVM), 2015.

60 E. D. Kuempel, L. M. Sweeney, J. B. Morris and A. M. Jarabek, *J. Occup. Environ. Hyg.*, 2015, **12**, S18–S40.

61 D. H. Bennett, T. E. McKone, J. S. Evans, W. W. Nazaroff, M. D. Margni, O. Jolliet and K. R. Smith, *Environ. Sci. Technol.*, 2002, **36**, 206A–211A.

62 M. A. J. Huijbregts, L. J. A. Rombouts, A. M. J. Ragas and D. van de Meent, *Integr. Environ. Assess. Manage.*, 2005, **1**, 181.

63 M. Huijbregts, M. Hauschild, O. Jolliet, M. Margni, T. McKone, R. K. Rosenbaum and D. van de Meent, *USEtox User Manual v1.01*, 2010.

64 K. E. Levine, R. A. Fernando, M. Lang, A. Essader and B. A. Wong, *Anal. Lett.*, 2003, **36**, 563–576.

65 K. S. Crump, *Fundam. Appl. Toxicol.*, 1984, **871**, 854–871.

66 K. S. Crump, *Risk Anal.*, 1995, **15**, 79–89.

67 H. Muhle, B. Bellmann, O. Creutzenberg, C. Dasenbrock, H. Ernst, R. Kilpper, J. C. MacKenzie, P. Morrow, U. Mohr, S. Takenaka and R. Mermelstein, *Fundam. Appl. Toxicol.*, 1991, **17**, 280–299.

68 K. P. Lee, H. J. Trochimowicz and C. F. Reinhardt, *Toxicol. Appl. Pharmacol.*, 1985, **79**, 179–192.

69 K. P. Lee, H. J. Trochimowicz and C. F. Reinhardt, *Toxicol. Appl. Pharmacol.*, 1985, **79**, 179–192.

70 U. Heinrich, R. Fuhst, S. Rittinghausen, O. Creutzenberg, B. Bellmann, W. Koch and K. Levsen, *Inhalation Toxicol.*, 1995, 7, 533.

71 E. D. Kuempel, C. L. Tran, V. Castranova and A. J. Bailer, *Inhalation Toxicol.*, 2006, **18**, 717–724.

72 *Risk Assessment of Chemicals: An Introduction*, ed. C. J. van Leeuwene and T. G. Vermeire, Springer, Netherlands, Dordrecht, 2nd edn, 2007.

73 E. Bermudez, J. B. Mangum, B. A. Wong, B. Asgharian, P. M. Hext, D. B. Warheit and J. I. Everitt, *Toxicol. Sci.*, 2004, 77, 347–357.

74 E. Demou, P. Peter and S. Hellweg, *Ann. Occup. Hyg.*, 2008, **52**, 695–706.

75 J. Sundell, H. Levin and D. Novosel, *Ventilation rates and health: report of an interdisciplinary review of the scientific literature*, Alexandria, 2006.

76 G. Oberdorster, J. Ferin and B. E. Lehnert, *Environ. Health Perspect.*, 1994, **102**, 173–179.

77 P. Hofstetter, T. Baumgartner and R. W. Scholz, *Int. J. Life Cycle Assess.*, 2000, **5**, 161–175.

78 M. D. Newman, M. Stotland and J. I. Ellis, *J. Am. Acad. Dermatol.*, 2009, **61**, 685–692.

79 N. Sadrieh, A. M. Wokovich, N. V. Gopee, J. Zheng, D. Haines, D. Parmiter, P. H. Siitonen, C. R. Cozart, A. K. Patri, S. E. McNeil, P. C. Howard, W. H. Doub and L. F. Buhse, *Toxicol. Sci.*, 2010, **115**, 156–166.

80 P. Filipe, J. N. Silva, R. Silva, J. L. Cirne de Castro, M. Marques Gomes, L. C. Alves, R. Santus and T. Pinheiro, *Skin Pharmacol. Physiol.*, 2009, **22**, 266–275.

81 N. A. Monteiro-Riviere, K. Wiench, R. Landsiedel, S. Schulte, A. O. Inman and J. E. Riviere, *Toxicol. Sci.*, 2011, **123**, 264–280.

82 F. Furukawa, Y. Doi, M. Suguro, O. Morita, H. Kuwahara, T. Masunaga, Y. Hatakeyama and F. Mori, *Food Chem. Toxicol.*, 2011, **49**, 744–749.

83 P. J. A. Borm, D. Robbins, S. Haubold, T. Kuhlbusch, H. Fissan, K. Donaldson, R. Schins, V. Stone, W. Kreyling, J. Lademann, J. Krutmann, D. Warheit and E. Oberdorster, *The potential risks of nanomaterials: a review carried out for ECETOC*, 2006, vol. 3.

84 M. Geiser, B. Rothen-Rutishauser, N. Kapp, S. Schürch, W. Kreyling, H. Schulz, M. Semmler, V. I. Hof, J. Heyder and P. Gehr, *Environ. Health Perspect.*, 2005, **113**, 1555–1560.

85 S. Fertsch-Gapp, M. Semmler-Behnke, A. Wenk and W. G. Kreyling, *Inhalation Toxicol.*, 2011, **23**, 468–475.

86 T. Jager, T. G. Vermeire, M. G. J. Rikken and P. Van der Poel, *Chemosphere*, 2001, **43**, 257–264.

87 J. A. Davis, J. S. Gift and Q. J. Zhao, *Toxicol. Appl. Pharmacol.*, 2011, **254**, 181–191.

88 S. Barlow, A. Chesson, J. D. Collins, A. Flynn, A. Hardy, A. Knaap, H. Kuiper, J. Larsen, D. Lovell, P. Le Neindre, J. Schlatter, V. Silano, S. Skerfving and P. Vannier, *EFSA J.*, 2009, **1150**, 1–72.

89 B. C. Allen, R. J. Kavlock, C. A. Kimmel and E. M. Faustman, *Fundam. Appl. Toxicol.*, 1994, **23**, 487–495.